Comparison of Cement- and Hydratable Alumina-Bonded Alumina-Spinel Materials for Steel Ladle Purging Plugs

B. Long, A. Buhr, I.-H. Jung, S. Jin, H. Harmuth, J. Dutton

This paper provides a summary of extended investigations performed on cement- and hydratable alumina bonded refractory materials for steel ladle purging plugs. The main wear factors of purging plugs are erosion due to intense stirring, corrosion by iron-oxide slag during oxygen lancing, and spalling due to thermal cycling. These were addressed in the investigation by theoretical thermodynamic evaluations using FactSage, mechanical property testing including hot modulus of rupture, and fracture behaviour testing using the wedge-splitting test. In addition, microstructural investigations were performed in order to explain differences in the material. The results provide a basis for assessment of different binder concepts especially for the purging plug application. These indicate the potential which hydratable alumina bonded materials could have in this area. Industrial and academic partners of the FIRE-network from three different continents have successfully cooperated in this study.

1 Introduction

Purging plugs in the steel ladle bottom are used for stirring the steel in the ladle during metallurgical treatment (Fig. 1). Their use is essential for the process. Clogged purging plugs cannot perform their function and therefore the hot surface of the purging plug is examined after each heat to ensure the gas channels/slits are open. In the case of residual steel or slag being present on the surface, pure oxygen is blown through a lance onto the surface to melt and wash any residue. During that process an iron oxide slag is formed which attacks the refractories at temperature above 2000 °C.

A low- or ultra-low-cement castable (LCC or ULCC) in the Al_2O_3–MgO–CaO system, based on corundum and with addition of spinel has become the standard solution for purging plugs over the past 20 years [1–5]. CaO-free hydratable alumina bonded castables (no cement, NCC) could be an

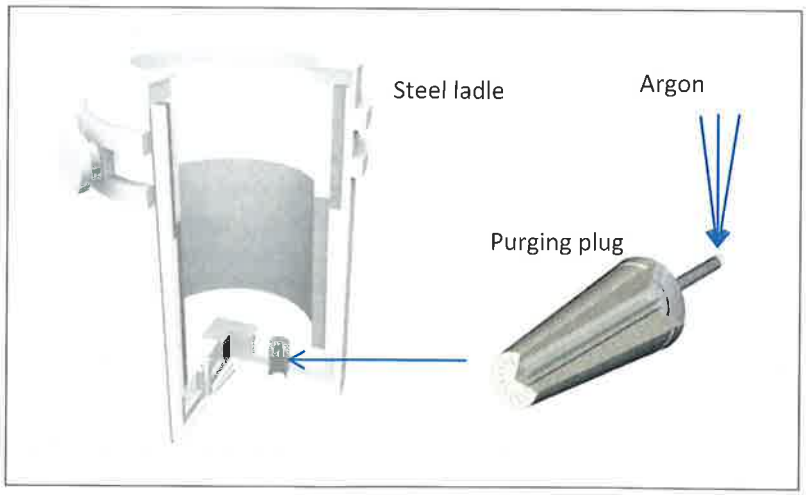

Fig. 1 Schematic picture of purging plug and steel ladle

Andreas Buhr
Almatis GmbH
Frankfurt
Germany

Bin Long
Almatis Qingdao
China

In-Ho Jung
McGill University Canada
Canada

Shengli Jin, Harald Harmuth
Chair of Ceramics
Montanuniversitaet Leoben
Austria

Jerry Dutton, Stourbridge
Great Britain

Corresponding author: *A.Buhr*
E-mail: Andus.Buhr@almatis.com

Keywords: Al_2O_3–MgO–CaO, FactSage analysis, cement bonded castable, no-cement castable, hydratable alumina, fracture behaviour, spalling, microstructure, steel ladle purging plug

Received: 29.04.2017
Accepted: 09.05.2017

Tab. 1 Composition of cement and hydratable alumina Alphabond 300 bonded castables (additives on top of 100 % sum)

Castable Recipe	C2S26	C5S26	C5S0	A4S26
Tabular alumina T60/T64	[%]	[%]	[%]	[%]
3–6 mm	25	25	20	25
1–3 mm	18	18	20	18
0,5–1 mm	6	6	10	6
0,2–0,6 mm			10	
0–0,5 mm	10	7		8
0–0,2 mm			15	
0–0,02 mm			7	
Spinel (AR 78)				
0,5–1 mm	7	7		7
0–0,5 mm	10	10		10
0–0,045 mm	9	9		9
Reactive alumina				
CL 370	13	13	13	13
Binder				
CA-14 M cement	2	5	5	
Alphabond 300				4
Additives				
ADS 3/ADW 1	1	1	1	1
Water demand	3,9	4,1	4,2	4,7

alternative for the purging plug application, because the absence of CaO would increase the resistance against iron oxide slag. In addition, the mechanical properties would change by replacing cement with hydratable alumina binder. This would influence the fracture behaviour. In industrial applications, the purging plugs are dried at temperatures around 400 °C or pre-fired at temperatures up to 1600 °C. This changes properties such as strength and fracture behaviour. In this regard, it is important to investigate the influences of pre-treatment temperature on the mechanical behaviour of purging plugs.

The main wear factors for purging plugs are erosion due to intensive stirring during the process, corrosion by aggressive iron-oxide rich slag at elevated temperatures during frequent cleaning operations of the clogged purging plug surface by "oxygen lancing", and spalling of layers from the hot face due to horizontal cracking caused by thermal cycling of purging plugs. New developments in steel metallurgy are concentrated around clean steel, alloy steel, tool steel, and higher manganese steel. This will make the working conditions for purging plugs even more challenging.

This paper provides a summary of investigations for comparing cement bonded with CaO-free hydratable alumina bonded refractory castables for the purging plug application, which were discussed in detail in previous publications [6, 7]. It would be very difficult or impossible to simulate the conditions that exist during "oxygen lancing" in practical tests in the laboratory. Therefore thermodynamic evaluations using FactSage were applied to assess differences between the binder concepts. The mechanical properties were tested, and the hot modulus of rupture (HMoR) especially provides a good indication regarding the erosion resistance of the material. Apart from the usual thermal shock resistance testing in the refractory industry, a more sophisticated fracture behaviour investigation via the wedge splitting test according to Tschegg [8] was carried out. In addition, the microstructure of the different materials after firing at 1650 °C was investigated in order to explain different mechanical behaviour after sintering.

2 Experimental

Three types of castable Al_2O_3–MgO–CaO, Al_2O_3–CaO, and Al_2O_3–MgO were produced using tabular alumina (T60/T64, Almatis), magnesium aluminate spinel (AR 78, Almatis), reactive alumina (CL 370, Almatis), and dispersing alumina (ADS 3, ADW 1, Almatis) as stated in Tab. 1. For the Al_2O_3–MgO–CaO and Al_2O_3–CaO systems, calcium aluminate cement (CA-14 M, Almatis) was used as binder. For the Al_2O_3–MgO castable, a hydratable alumina (Alphabond 300, Almatis) was used as the binder.

This paper reports results for 2 % or 5 % cement, or 4 % hydratable alumina in the formulation. Results with higher cement contents and lower or higher hydratable alumina contents were reported in a previous paper [6].

Raw materials were dry mixed in a Hobart mixer for 1 min and then wet mixed after adding the water. The wet out time for the two types of mixes was different. For the cement bonded mix, the wet out time was around 40 s and wet mixing time a total of 4 min. For the Alphabond 300 mix, the wet out time was 2 min, resulting in a longer wet mixing time of a total of 6 min. Longer mixing time for the hydratable alumina containing mix is important for both the laboratory test and in practical application. Insufficient mixing may, in practice, cause overdosing of water, which will significantly deteriorate the castable. In industrial applications, 2–4 % of Alphabond 300 is recommended for such mixes to avoid a too high water demand with higher Alphabond 300 contents.

All castables were adjusted by appropriate water addition to achieve a vibration flow value of around 200 mm. This is the figure that is typically required for proper installation. Mixes were cast into moulds 40 mm × 40 mm × 160 mm for the testing of general physical properties, and 100 mm × 100 mm × 75 mm for the wedge splitting test. Smaller moulds of 25 mm × 25 mm × 125 mm were used for casting sample bars for HMoR testing [9]. After curing and drying the sample bars were then fired at different temperatures with a holding time of 5 h. The cold modulus of rupture (CMoR), cold crushing strength (CCS), bulk density, open porosity and permanent linear change were then tested.

Microstructures of the samples were examined using a scanning electron microscope (FEI-SIRION, operated at 5 kV) equipped with an energy-dispersive X-ray spectrometer. The mineral phases were identified by X-ray diffraction (XRD; Rigaku D/DMAX-RB) using Cu K_α radiation (40 kV, 20 mA, λ = 0,15406 nm) in the 2θ angular range 10–100° and with a scan speed of 2°/min.

The wedge splitting test (Fig. 2) was conducted at Montanuniversitaet Leoben, and three samples of each material were used in order to prove repeatability. The applied wedge splitting test is suitable for determining the specific fracture energy of refractories by using specimens with sufficiently large dimensions [10, 11]. After the wedge splitting test, the specific fracture energy G'_f and nominal notch tensile strength σ_{NT} can be obtained according to eq. 1 and eq. 2.

The Young's moduli of the samples were measured by resonance frequency of damping analysis (RFDA, IMCE/BE) at Montanuniversitaet Leoben. The samples were cast into bars of 25 mm × 25 mm × 125 mm. After curing at 20 °C for 24 h and drying at 110 °C for 24 h, all samples were pre-fired at 350 °C for 5 h. Young's moduli of the samples were measured after pre-firing at 350, 1250 and 1500 °C respectively.

The equation used to calculate the characteristic length (l_{ch}) is shown in eq. 3, where G'_f represents the specific fracture energy, E is Young's modulus, and σ_{NT} is the nominal notch tensile strength [10, 11]. Thermal shock resistance parameter R'''' can be calculated according to eq. 4, where γ is the specific surface fracture energy [11–13]. As γ is the energy relative to the double area of the projection of the fracture surface, R'''' equals $l_{ch}/2$. In the present paper, l_{ch} is used to compare the thermal shock resistance of investigated materials.

$$G'_f = \frac{1}{A}\int_0^{\delta_{nlt}} F_H \, d\delta \qquad \text{(eq. 1)}$$

$$\sigma_{NT} = F_{max}(1 + 6\gamma/h)/bh \qquad \text{(eq. 2)}$$

$$l_{ch} = G'_f E/\sigma^2_{NT} \qquad \text{(eq. 3)}$$

$$R'''' = \gamma E/\sigma^2_{NT} \qquad \text{(eq. 4)}$$

For thermal shock resistance testing, quenching in water was carried out according to the Chinese national standard YB/T 376.1-1995 [14]. Samples were pre-fired at 400 and 1650 °C, respectively with a holding time of 5 h. Samples were held at 1100 °C for 20 min and then immersed into running water for 3 min. The above process was considered as one cycle. Residual CMoR was tested after one and three cycles, and compared to the starting CMoR.

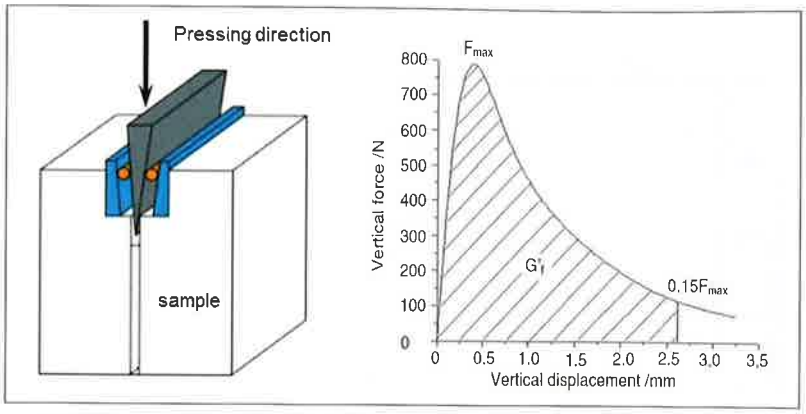

Fig. 2 Schematic of the wedge-splitting test (left), and a typical load–displacement curve (r.) [11]

3 Thermodynamic analysis by FactSage

3.1 Overview of the refractory and slag system

For purging plug refractory materials in general, the chemical composition will be very close to the angle of corundum (α-Al_2O_3) in the ternary phase diagram Al_2O_3–MgO–CaO [15] due to the low amounts of CaO (low or ultra-low cement castable) and MgO (10~20 % of spinel (MgO·Al_2O_3, MA) equals to 2~5 % MgO), and the high amount of corundum. In thermodynamic equilibrium, the phases of the purging plug at a high service temperature in the range 1600–1700 °C will be corundum, spinel, and CaO·6Al_2O_3 (CA_6), with the peritectic melting point at 1850 °C [16, 17]. Göbbels et al. [18] and Iyi et al. [19] reported the two ternary compounds $C_2M_2A_{14}$ and CM_2A_8 as metastable phases at high temperature in the ternary system. The existence of metastable ternary compounds was confirmed by the studies of De Aza et al. [17].

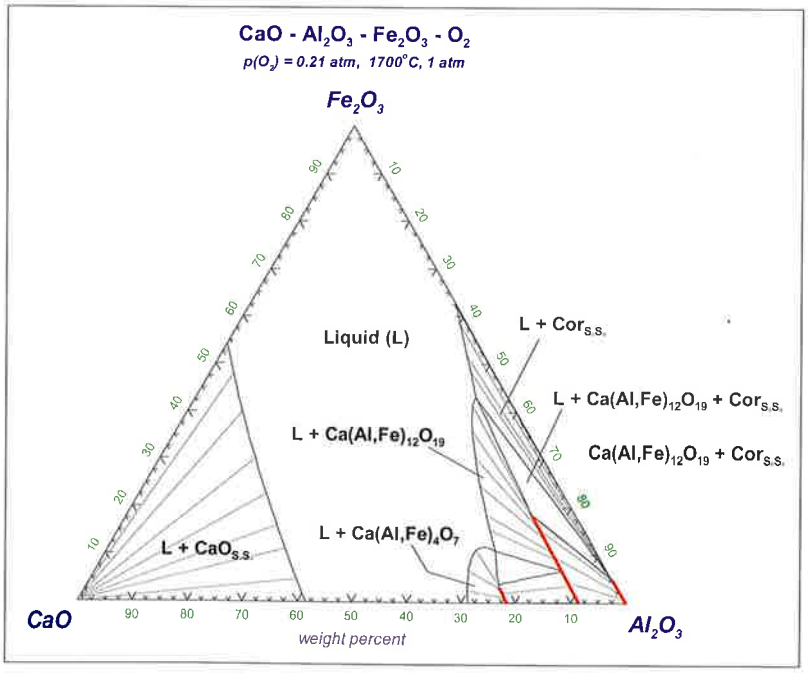

Fig. 3 Isothermal phase diagram of the system Al_2O_3–Fe_2O_3–CaO in air at 1700 °C

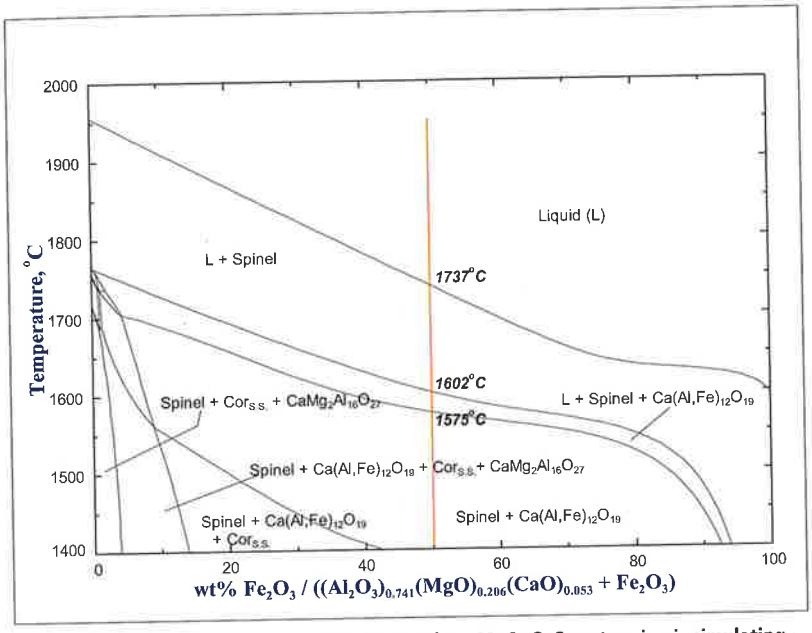

Fig. 4 Calculated phase diagram of the Fe_2O_3–Al_2O_3–MgO–CaO system in air simulating the chemical reaction between C5S26 refractory (matrix) and iron oxide

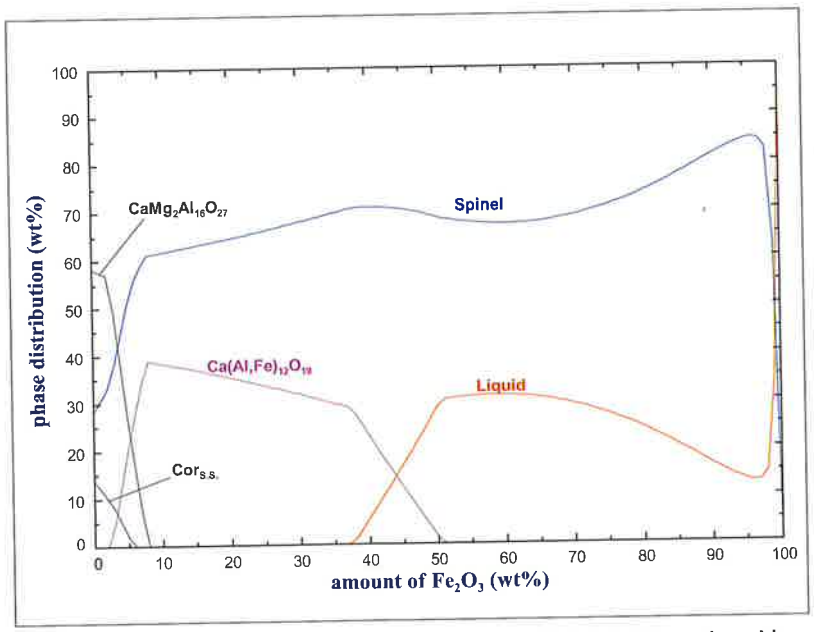

Fig. 5 Evolution of the phase distribution of C5S26 refractory (matrix) in reaction with iron oxide in air calculated at 1600 °C

After each heat in the steel ladle, some residual liquid steel will remain on the bottom until the ladle is tilted. This steel can freeze at the top of the purging plug, or may infiltrate into the slits of the purging plug. Oxygen lancing is a conventional way to melt and blow away the residual steel on top of the purging plug and to open the slits of the purging plug. In the oxygen lancing process, the hot iron will react with oxygen to form iron oxide in a strongly exothermic reaction, e.g. for FeO $\Delta_f H^0$ is –272,0 kJ/mol [20]. FeO_x will react with refractory at very high temperatures. Therefore it is necessary to study the chemical reaction between the iron oxide and the purging plug material.

Depending on the oxidation state of iron, the phases spinel, corundum, and CA_6 can form iron containing solid solutions with Fe^{2+} and/or Fe^{3+} to replace Mg^{2+} and Al^{3+} respectively. The solubility of iron oxide in corundum depends on the atmosphere and temperature. At 1 atm O_2 pressure around 20 % iron oxide can be incorporated into the corundum lattice at 1490 °C [15]. Melting temperatures of these solid solutions decrease by increasing iron oxide content. Another dominant reaction is the spinel formation by reaction of iron oxide (Fe^{2+}) with corundum, so that $FeAl_2O_4$ spinel (hercynite) becomes the dominant phase instead of corundum with increasing iron oxide content. $FeAl_2O_4$ melts at 1780 °C [15].

Thermodynamic calculations were made using the FactSage 6.4 version with FToxid and FACTPS database at McGill University Canada (Fig. 3–9).

The phase diagram of the Al_2O_3–Fe_2O_3–CaO ternary system in air at 1700 °C is calculated in Fig. 3. There is CA_2 solution ($Ca[Al,Fe]_4O_7$), CA_6 solution ($Ca[Al,Fe]_{12}O_{19}$) and corundum solution ($[Al,Fe]_2O_3$) in this system. As can be shown, the addition of iron oxide can expand the liquid area at 1700 °C. CA_6 solid solution and corundum solid solution co-exist in the small area close the corundum angle. Based on the above analysis it can be concluded that, at 1700 °C, iron oxide has a severe corrosive effect on the lime containing refractory system.

3.2 The effect of iron oxide on the refractory systems Al_2O_3–MgO–CaO and Al_2O_3–MgO

The specific composition of recipe C5S26 was taken as an example for thermodynamic analysis. The bulk chemistry of the castable is 92,8 mass-% Al_2O_3, 5,7 mass-% MgO, and 1,5 mass-% CaO. During slag attack on refractories, coarse aggregates are relatively inert when compared to the fine matrix material, due to much lower porosity and fewer chemical compounds. The lime-containing cement is only present in the matrix. Therefore, all aggregates above 0,5 mm were excluded for the thermodynamic calculations. The matrix material includes tabular alumina fines, alumina magnesia spinel, reactive alumina and calcium aluminate cement. The chemical composition for the matrix material is 87,1 mass-% Al_2O_3, 9,5 mass-% MgO and 3,4 mass-% CaO. Transforming into mole composition, the components are 74,1 mol-% Al_2O_3, 20,6 mol-% MgO and 5,3 mol-% CaO.

Assuming that a pure iron oxide is formed during oxygen lancing, a phase calculation for the effect of iron oxide on the Al_2O_3–

MgO–CaO ternary system is plotted in Fig. 4. The weight percentage of Fe_2O_3 to the combination of Fe_2O_3 and refractory, is presented as the X-axis. In this system, the phases are corundum solid solution (corundum ss), $(Mg, Fe)(Al, Fe)_2O_4$ solid solution (spinel ss), CA_6 solid solution (CA_6 ss), and $CaO{\cdot}2MgO{\cdot}8Al_2O_3$. By increasing the content of iron oxide, the stability range of the above mentioned phases decreases and the liquidus temperature falls. At a fixed amount of Fe_2O_3, the amount of solid phases decreases by increasing the temperature, due to liquid phase formation.

The reaction of purging plug refractory and iron rich slag occurs at the interface of the hot face of the material or in the slit area. Here, the ratio of slag to slag+refractory can be assumed to be 50 %, as shown by the red line in Fig. 4.

The co-existing phases are spinel solid solution and CA_6 solid solution at temperatures below 1575 °C. Above this temperature in addition to these two phases, liquid phase also appears. At 1602 °C, melting of the CA_6 solid solution is complete. The spinel solid solution, the last remaining solid phase, continues to melt with increasing temperature and is completely molten at 1737 °C.

The equilibrium phase distribution at 1600 °C is plotted in Fig. 5. Solid phases include corundum, CM_2A_8, CA_6 ss, and spinel ss. The metastable phase CM_2A_8 transforms to CA6 ss and spinel ss at Fe_2O_3 contents greater than 2 mass-%. Corundum reacts with iron oxide and the magnesium aluminate spinel forming spinel ss, and disappears at 6 mass-% Fe_2O_3. CA_6 ss disappears at around 50 mass-% Fe_2O_3, which is in line with the above analysis. The spinel ss phase is the dominating phase over the entire composition range of Fe_2O_3 until it approaches the composition of magnetite (Fe_3O_4). Liquid phase appears at 37,5 mass-% Fe_2O_3. At 50 mass-% Fe_2O_3, the phase composition is 28 mass-% liquid and 69 mass-% spinel solid solution, and only 3 mass-% CA_6 solid solution.

Fig. 6 shows the Al_2O_3–MgO–CaO–Fe_2O_3 phase calculation at 1700 °C. The stability range of spinel ss with regard to melting has decreased significantly. Liquid phase has already appeared at 6 mass-% Fe_2O_3. At 50 mass-% Fe_2O_3, the phase composition is 75,5 mass-% liquid, and 22,5 mass-% spinel ss, much lower than the 69 mass-% spinel ss existing at 1600 °C.

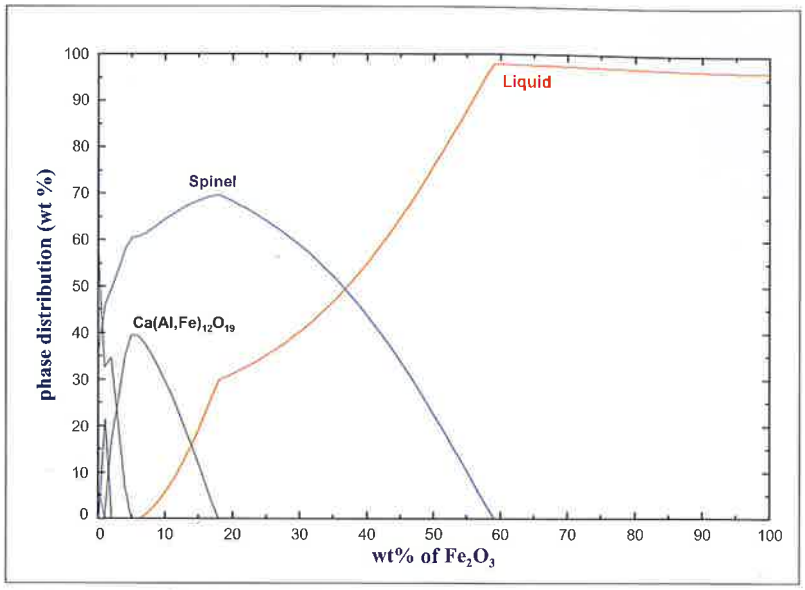

Fig. 6 Evolution of the phase distribution of C5S26 refractory (matrix) in reaction with iron oxide in air calculated at 1700 °C

To evaluate the CaO effect on the phase relationships of the above Al_2O_3–MgO–CaO–Fe_2O_3 quaternary system, the CaO component is completely eliminated as shown in Fig. 7. The percentage of MgO (from spinel raw material) remains the same. The specific composition of recipe A4S26 was taken as an example for thermodynamic analysis. The bulk chemistry of the castable consists of 94,3 mass-% Al_2O_3 and 5,7 mass-% MgO. The matrix material includes 79 mol-% Al_2O_3 and 21 mol-% MgO. In this case, it becomes a ternary system of Al_2O_3–MgO–Fe_2O_3. The co-existing solid phases are corundum ss and spinel ss. By increasing the Fe_2O_3 content the above stability range of both solid solutions, with regard to melting, decreases. At a fixed amount of 50 mass-% Fe_2O_3 (red line in Fig. 7), spinel ss and corundum ss will co-exist below 1454 °C. From 1454 °C to 1665 °C, spinel ss is the single phase in the system,

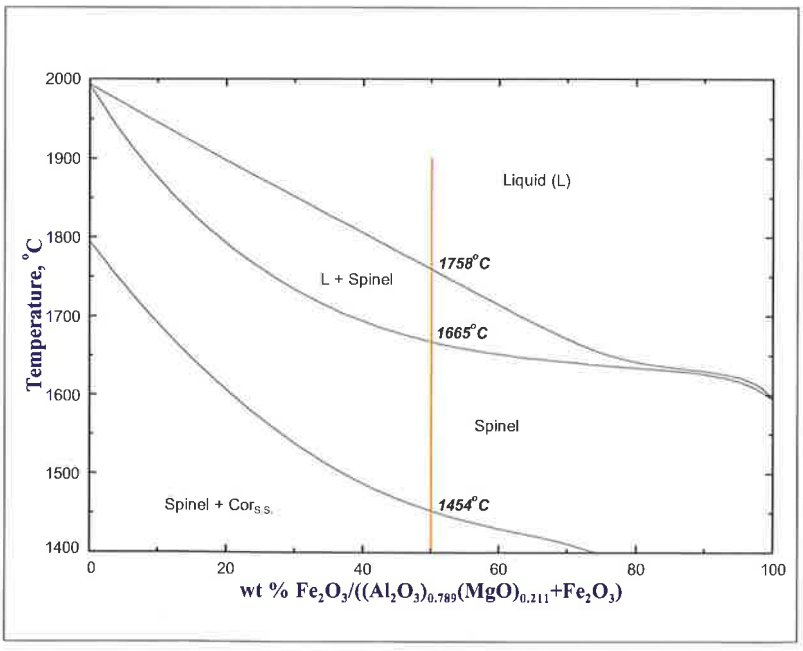

Fig. 7 Calculated phase diagram of the Fe_2O_3–Al_2O_3–MgO system in air simulating the chemical reaction between A4S26 refractory (matrix) and iron oxide

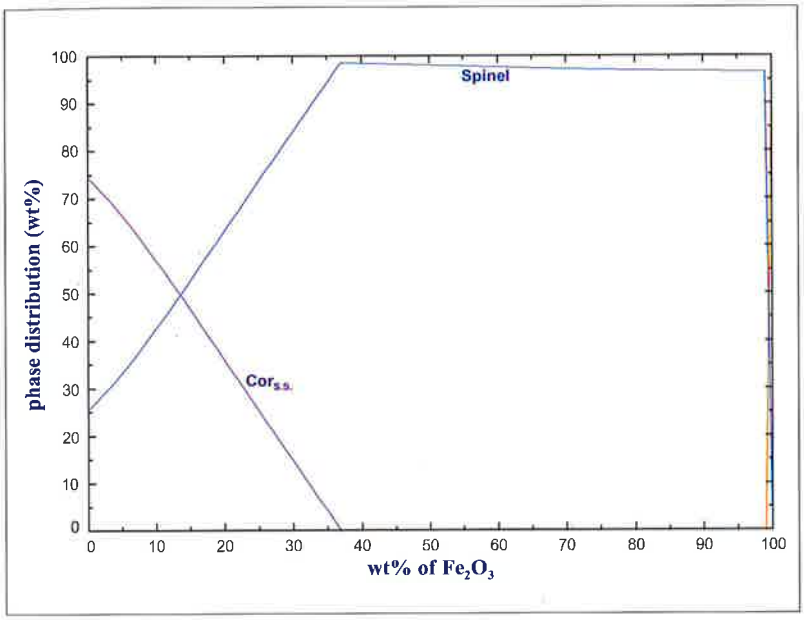

Fig. 8 Evolution of the phase distribution of A4S26 refractory (matrix) in reaction with iron oxide in air calculated at 1600 °C

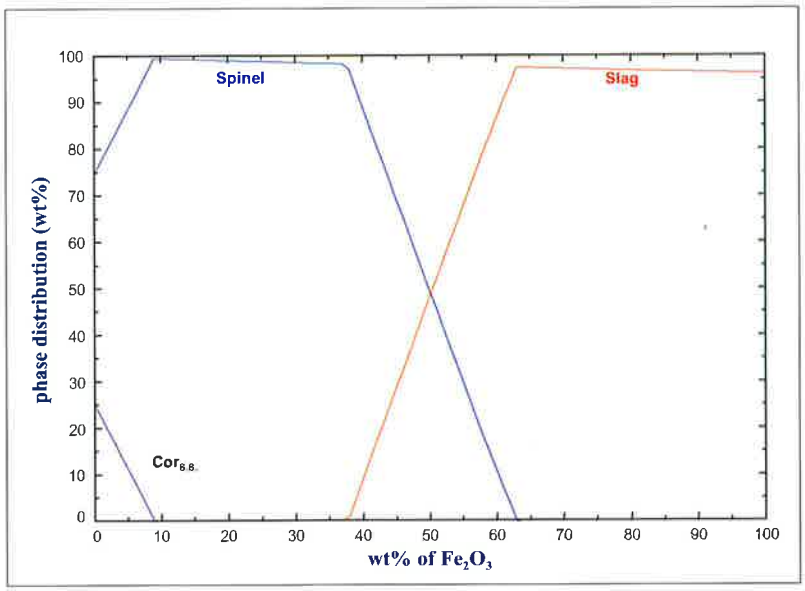

Fig. 9 Evolution of the phase distribution of A4S26 refractory (matrix) in reaction with iron oxide in air calculated at 1700 °C

meaning the corundum reacts with iron oxide to form spinel solid solution. Above 1665 °C, liquid starts to appear. As the temperature increases to 1758 °C, spinel ss becomes completely molten. As with the lime containing system earlier, the phase diagram is plotted at 1600 °C (Fig. 8) and at 1700 °C (Fig. 9). At 1600 °C, there is no liquid phase in the system. Corundum ss and spinel ss coexist until the Fe_2O_3 content increases above 21 mass-%, because the corundum ss forms spinel ss by reaction with iron oxide.

At 1700 °C (Fig. 9), the corundum phase disappears at Fe_2O_3 content of 8 mass-%. In this case, spinel ss starts melting at 37,5 mass-% Fe_2O_3. At an iron oxide content of 50 mass-%, there is 50 mass-% liquid phase in the system. Further increase in Fe_2O_3 content leads to complete melting of the spinel ss at 63,5 mass-% Fe_2O_3.

In order to compare the two systems of Al_2O_3–MgO–CaO–Fe_2O_3 and Al_2O_3–MgO–Fe_2O_3, Tab. 2 consolidates important results from the thermodynamic evaluation. It shows the calcia-free system has a clear advantage to the system with calcia. The onset temperature of liquid phase for the calcia-free system is higher, which indicates higher refractoriness. Furthermore, the liquid content of the calcia-free system at 1600 °C and 1700 °C is clearly lower than in the system with calcia, which would indicate better anti-corrosion characteristics. In general, the system of Al_2O_3–MgO can be considered better than the system Al_2O_3–MgO–CaO regarding resistance against iron oxide slag attack.

Tab. 2 Thermodynamic analysis on the effect of iron oxide on the system Al_2O_3–MgO–CaO and Al_2O_3–MgO in air at a defined chemical composition (refractory matrix as basis, see text)

	Al_2O_3–MgO–CaO	Al_2O_3–MgO
Onset temperature of liquid phase at 50 mass-% Fe_2O_3	1575 °C	1665 °C
Liquid phase content at 1600 °C and 50 mass-% Fe_2O_3	28 mass-%	0
Liquid phase content at 1700 °C and 50 mass-% Fe_2O_3	75,5 mass-%	50 mass-%

3.3 Review analysis on used steel ladle purging plug

A used purging plug based on corundum/spinel low cement castable was taken as an example for review analysis. The original height of the purging plug was 420 mm, with a top diameter of 120 mm and bottom diameter of 180 mm. There were two rows of slits in the purging plug, with 10 in the inner area and 20 in the outer area. After 25 heats (including ladle furnace and vacuum degassing treatment) of, in total, about 2000 min, the residual height of the purging plug was reduced to 250 mm, with a concave shape in the hot face area. A sample of the hot face of the purging plug was taken for SEM analysis.

Fig. 10 shows the transition zone of infiltrated area and non-infiltrated area. The bright phase areas are infiltrated steel. The lighter grey areas beside the infiltrated steel were verified as spinel solid solution. The EDS results indicate FeO rich spinel ss with minor content of MgO. Due to the high amount of liquid steel and iron-rich slag in-

filtrated into the refractory material and the high temperatures during oxygen lancing, the iron oxide can easily react with magnesia aluminate spinel and corundum to form the spinel solid solution. According to Fig. 4, such iron rich spinel solid solution is thermodynamically much more stable than any other phase in the system. The darker grey phase beside spinel ss and infiltrated steel is CA_6, and does not show a solid solutioning with Fe_2O_3 according to the EDS results.

4 Results and discussion

4.1 Mechanical properties

Data of the test castables pre-fired at 1650 °C are given in Tab. 3. More data for these properties and a discussion of the differences at different temperatures are given in a previous paper [6]. At 1650 °C sintering shrinkage occurs for all test castables regardless of the binder. The open porosity of the hydratable alumina castable is about 25 % higher when compared to the cement bonded castables. This can be explained by a higher mixing water demand (4,7 % of the hydratable alumina vs. 3,9 % to 4,2 % for the cement bonded mixes) due to the very high specific surface area, 250–300 m²/g, of the Alphabond 300 which absorbs water. The CMoR and CCS results are given in Fig. 11–12. The strength levels vary depending upon temperature. The curing strength at 20 °C is the lowest.

During "drying" at 110 °C further hydration takes place and the strength increases accordingly, because this temperature is too low to remove all pore water from these dense and low permeability castables. Tempering at 350 °C, where most of the water is removed, in general does not change the strength level. The strength level of the ultra-low cement castable C2S26 and hydratable alumina castable A4S26 is lower when compared to the higher cement content of C5S26 and C5S0 (LCC).

It is interesting to see that the hydratable alumina mix has slightly higher strength after drying and tempering than the ULCC. At 1000 °C, the hydrates formed by the cement have decomposed and weak ceramic sintering has started. Also for the hydratable alumina binder the hydrates that formed have now decomposed. However, a difference can be seen as the strength level of

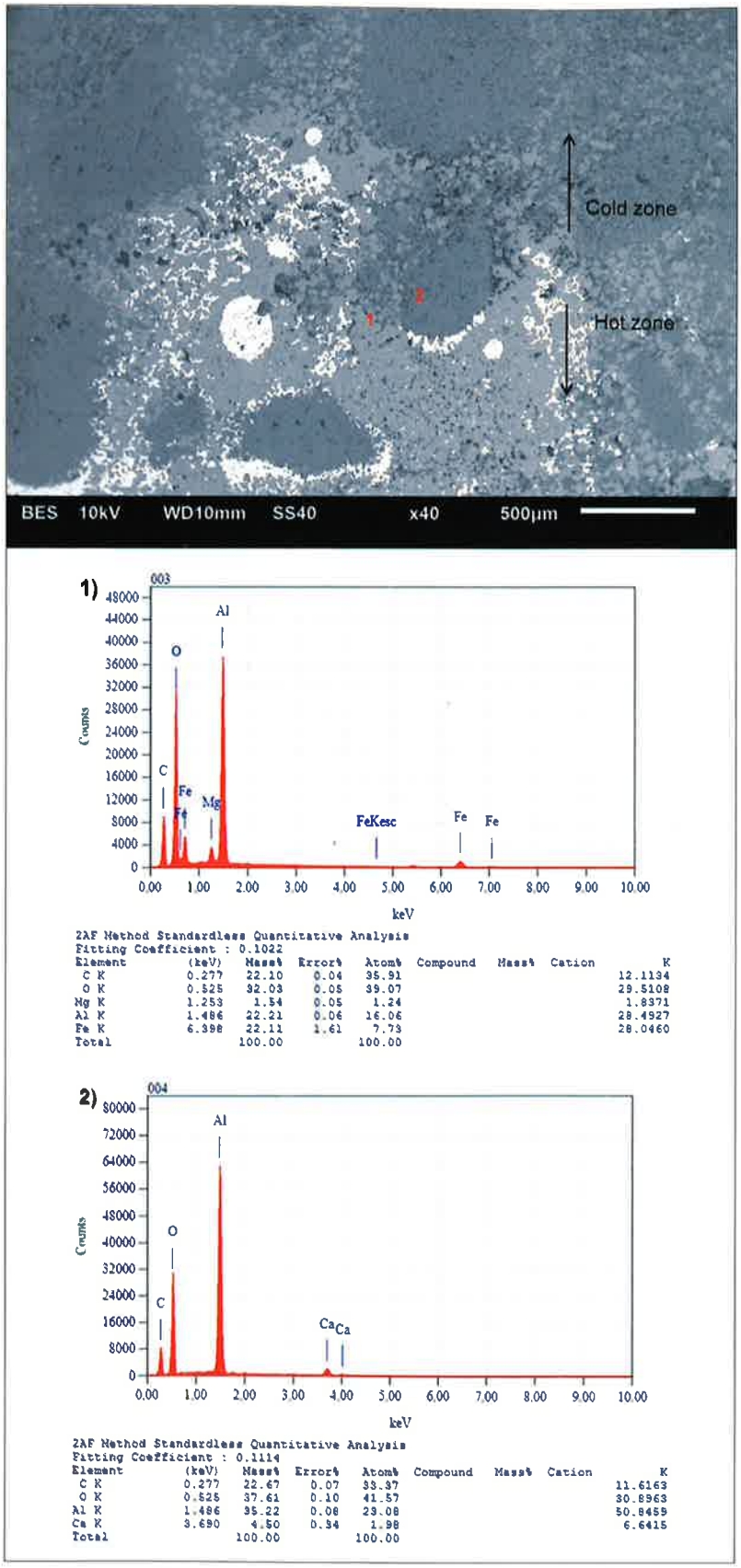

Fig. 10 SEM and EDS analysis on used purging plug: spinel solid solution (light grey phase, #1, EDS analysis top); 2 indicates CA6 (dark grey phase, #2, EDS analysis bottom; bright phase is infiltrated steel

Tab. 3 Open porosity, bulk density and permanent linear change of cement bonded castables after firing at 1650 °C/5 h

Castable	C2S26	C5S26	C5S0	A4S26
Bulk density [g/cm³]	3,20	3,16	3,20	3,13
Open porosity [%]	12,1	12,3	11,8	16,3
Permanent linear change [%]	–0,42	–0,38	–0,65	–0,34

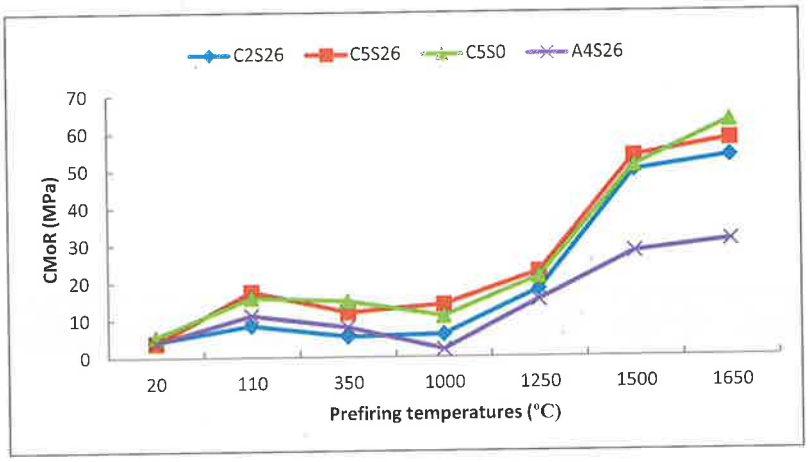

Fig. 11 Cold modulus of rupture at different pre-firing temperatures

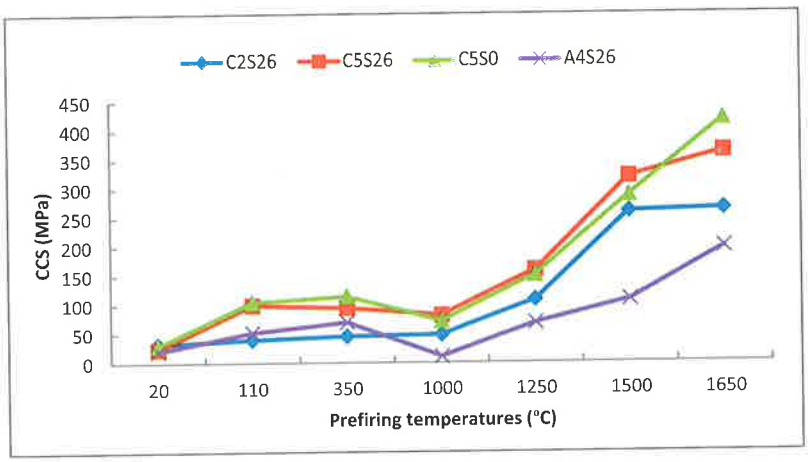

Fig. 12 Cold crushing strength at different pre-firing temperatures

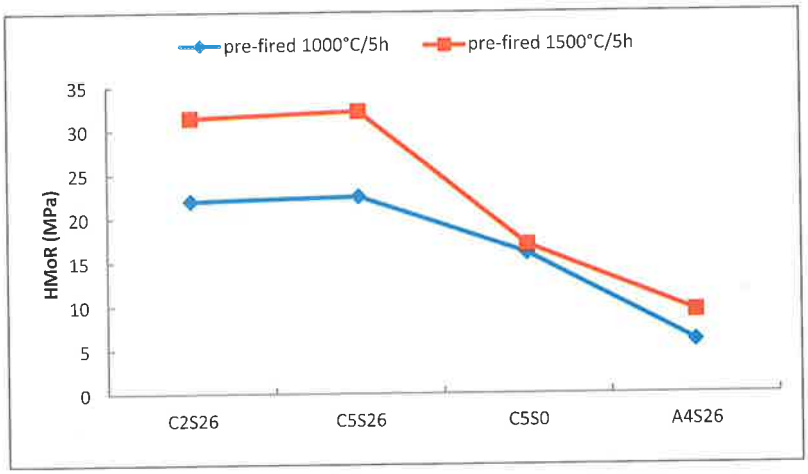

Fig. 13 HMoR after pre-firing at 1000 °C/5 h and 1500 °C/5 h, respectively (tested at 1500 °C/0,5 h)

the hydratable alumina mix is clearly lower at 1000 °C. Obviously a higher temperature is needed to enable sintering in this system, e.g. 1250 °C as shown in Fig. 11–12. High firing temperatures such as 1500 °C and 1650 °C lead to clear strength increases. The strength level of the cement bonded mixes is about double of the hydratable alumina bonded mix, regardless whether the cement content is 2 % or 5 %.

For industrial application the strength level of the Alphabond 300 castable fired at 1250 °C or higher is considered sufficient. When comparing different cement contents it appears that the cement content does not influence the sintered strength at high temperatures. However, when comparing the ULCC with the no-cement castables it becomes apparent, that even a small amount of cement has a clear effect on the sintered strength at high temperatures. All castables have the same amount of reactive alumina in the matrix.

During the production of a purging plug, sufficient curing strength is needed in order to provide adequate mechanical strength for the de-moulding, handling, and transportation of the green purging plug. The drying strength at 350–400 °C is also important, because most purging plugs in Europe are tempered in that temperature range before delivery to the steel works. In China, purging plugs are generally already pre-fired at high temperature prior to application in the steel ladle. Strength at 1000 °C might be irrelevant for those purging plugs which are pre-fired at high temperatures, for example 1600 °C, when the ceramic bond has already formed. However it would be relevant to those tempered at lower temperatures of around 400 °C, because each purging plug goes through a temperature of around 800~1000 °C during pre-heating or operation, and the purging plug could fail if the mechanical strength is insufficient. Strength at 1500 °C and 1650 °C is normally perceived as critical to indicate whether a good ceramic bond forms while the material still retains volume stability. However, too high strength could possibly induce low thermal shock resistance.

HMoR results after 5 h pre-firing at 1000 °C and at 1500 °C are shown in Fig. 13. The test was conducted at 1500 °C after a holding time of 30 min. The HMoR was higher when the samples were pre-

fired at 1500 °C because sintering took place, forming a stronger ceramic bond. For C5S0 without spinel this effect is less pronounced. When comparing C2S26 and C5S26, HMoR appears to be almost independent of the cement content. Further investigations reported in a previous paper [6] show, that higher cement content such as 10 % appears to reduce HMoR, and for varying Alphabond 300 contents between 2–6 % HMoR does not change significantly. HMoR is an important factor which can affect the performance of a purging plug. Higher HMoR is beneficial for the erosion resistance of a purging plug under working conditions, where erosive attack is strong due to the stirring of the steel especially at and around the purging plug. The cement bonded castables show good HMoR values. These are regarded as being adequate for the practical application of the purging plug.

The HMoR level of ultra-low cement castable C2S26 and low cement castable C5S26 is around three to four times higher than Alphabond 300 bonded castable. This is attributed to overall stronger sintering reactions in the cement bonded mixes including the formation of new phases such as CA_6. The clearly higher HMoR of cement bonded castables even at a low cement content of only 2 % (C2S26) is a clear advantage versus the no-cement castables with hydratable alumina when considering the purging plug application, where high erosion resistance is required.

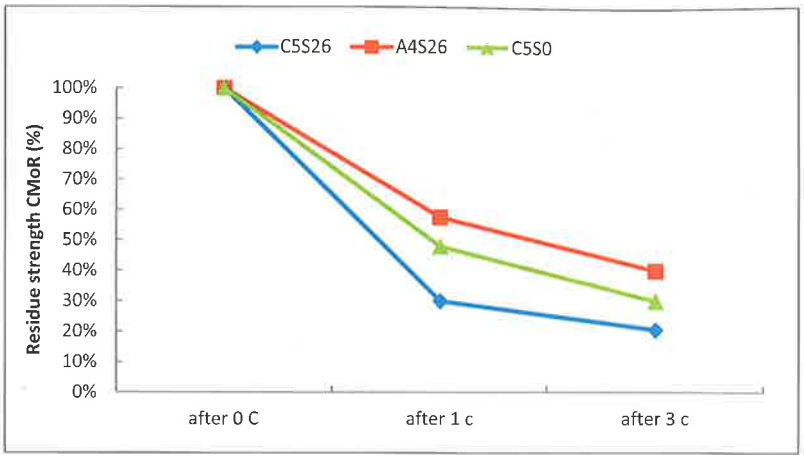

Fig. 14 Residue strength CMoR [%] after 1 and 3 water quenches (pre-fired at 400 °C/5 h)

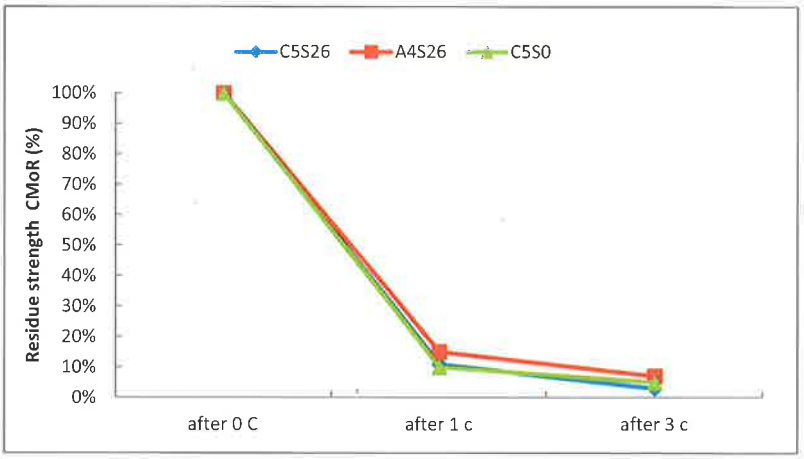

Fig. 15 Residue strength CMoR [%] after 1 and 3 water quenches (pre-fired at 1650 °C/5 h)

4.2 Thermal shock resistance

The results of thermal shock resistance testing by water quenching are shown in Fig. 14–15. The relative strength losses after one and three cycles are lower for 400 °C pre-firing when compared to 1650 °C pre-firing. At 400 °C pre-firing, the residual CMoRs are 30–58 %, whereas at 1650 °C pre-firing, they are only 10–15 %. The residual CMoR in relative terms is higher for the no-cement castable than for the cement bonded castables.

This would in general indicate a higher thermal shock resistance for the materials pre-fired at the low temperature, and also a higher resistance for the no-cement castable when compared to the cement bonded castables. However, the lower starting strength level of the no-cement material when compared to the cement bonded material also needs to be taken into account, especially at 350 °C (8 MPa vs. 18 MPa).

4.3 Wedge splitting and Young's modulus test results

Fracture curves of castables pre-fired at 350 °C for 5 h are shown in Fig. 16. The results show that C5S0 and C5S26 have higher maximum vertical forces than A4S26. C5S0 shows slightly higher vertical force than C5S26 which is in line with slightly higher strength values as given in Fig. 11–12.

Fracture curves of castables pre-fired at 1250 °C for 5 h and at 1500 °C for 5 h are shown in Fig. 17–18, respectively. These results show that castables C5S26 and C5S0 exhibit higher vertical forces than the no-cement castable A4S26. The castable C5S26 exhibits the highest vertical force. Compared to the curves of samples pre-fired at a lower temperature (Fig. 16), the curves for C5S26 and C5S0 in Fig. 17–18 are much steeper during the descending load process, which indicates greater brittle cracking in the castables [8]. In the case of the no-cement bonded castable A4S26 in Fig. 17–18, the curves are very similar to that in Fig. 16. The slopes of the curves of A4S26 are lower than those of the cement bonded castables, suggesting a more gentle fracture process and less brittle behaviour of the A4S26 sample.

The specific fracture energy of the castables pre-fired at different temperatures is displayed in Fig. 19. These values are calculated from the integral of the load/displacement curves in Fig. 16–18, and divided by the fracture surface projection area, as previously discussed. The results show, that as temperature increases, the specific fracture energy of C5S26 and C5S0 increases. This

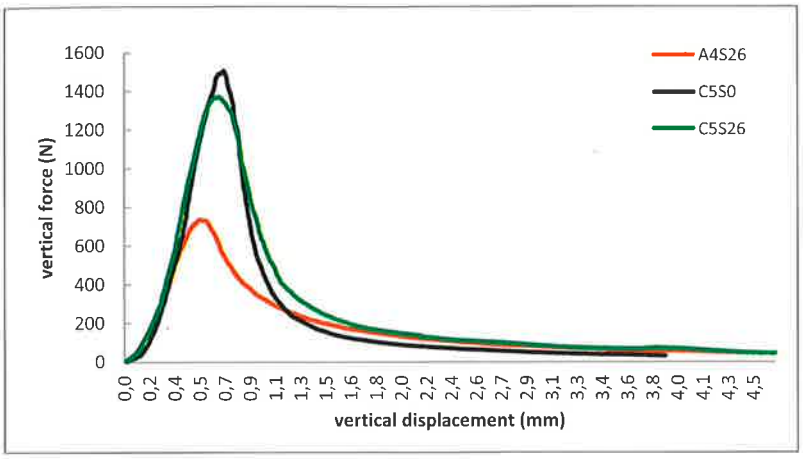

Fig. 16 Load/displacement curves of the castables pre-fired at 350 °C for 5 h

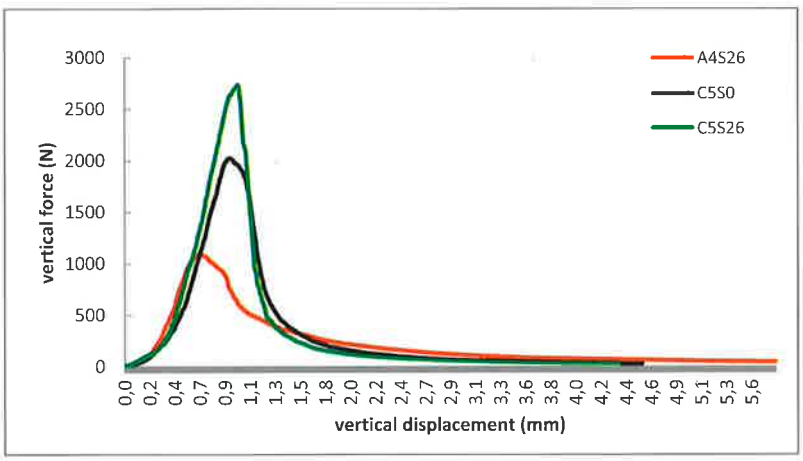

Fig. 17 Load/displacement curves of the castables pre-fired at 1250 °C for 5 h

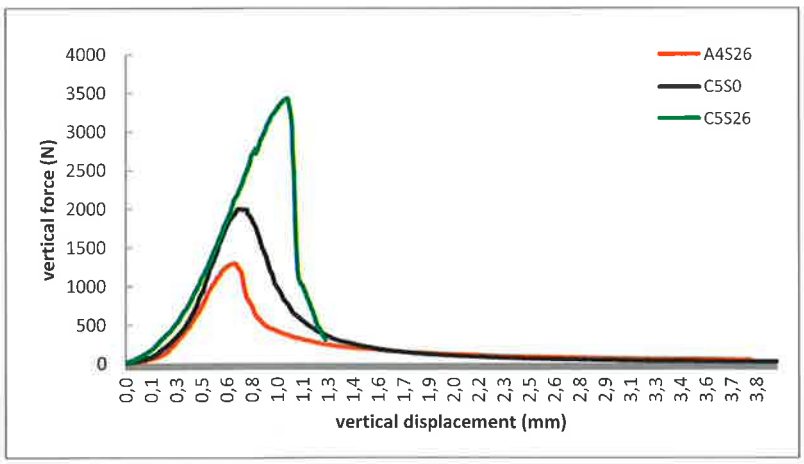

Fig. 18 Load/displacement curves of the castables pre-fired at 1500 °C for 5 h

increase in the specific fracture energy is a consequence of the increase in the mechanical strength of the castables at higher temperatures, which results in a stronger bonding effect. By contrast, in the case of A4S26, the fracture energy increases up to 1250 °C and then decreases at 1500 °C. This is attributed to brittle cracking promoted after high temperature treatment as seen in Fig. 17–18.

The nominal notch tensile strength of castables after pre-firing at different temperatures is shown in Fig. 20. The relationship of the σ_{NT} value with respect to the pre-firing temperature is similar to that of the cold modulus of rupture and cold crushing strength, as shown in Fig. 11–12. Namely, as temperature increases, σ_{NT} increases accordingly. In addition, the no-cement castable A4S26 exhibits a lower σ_{NT} than the other two castables at various temperatures.

The Young's modulus results are shown in Fig. 21. The Young's modulus of a material is normally proportional to its mechanical strength. Therefore, samples pre-fired at higher temperatures demonstrate higher E values because the CMOR and CCS are greatly enhanced at higher temperatures, as observed in Fig. 11–12. Therefore, a substantial increase of the Young's moduli of all three materials is observed after the materials were pre-fired at 1500 °C.

The characteristic length calculated by eq. 3 is shown in Fig. 22. The results show that the three castables perform differently at various pre-firing temperatures. The no-cement material A4S26 exhibits the highest l_{ch} value among the tested materials, irrespective of the pre-firing temperature, mainly because the sample exhibits the lowest nominal notch tensile strength σ_{NT}, as l_{ch} is inversely proportional to the squared σ_{NT}. Therefore, the castable bonded with hydratable alumina displays the least brittleness compared to materials with a cement bond. In addition, the l_{ch} value of the A4S26 decreases as pre-firing temperature increases. These results suggest that higher pre-firing temperatures adversely affect the thermal shock resistance. However, without a higher pre-firing temperature, the no-cement castable may fail because of low mechanical strength at 1000 °C. Therefore, the pre-firing temperature of approximately 1250 °C for the Alphabond 300 bonded castable would possibly be applicable for optimising both mechanical strength and fracture resistance.

Among the three materials which were investigated, the material with cement and spinel (C5S26) showed the lowest l_{ch} values at 1250 °C and 1500 °C. The main contributions to these values originate from the higher nominal notch tensile strengths of C5S26.

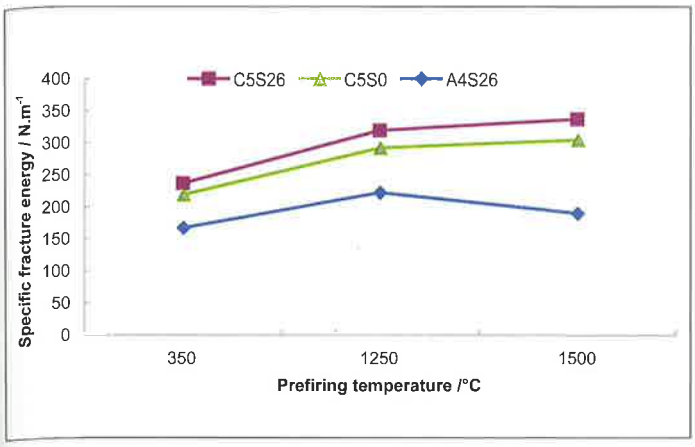

Fig. 19 Specific fracture energy of castables pre-fired at different temperatures

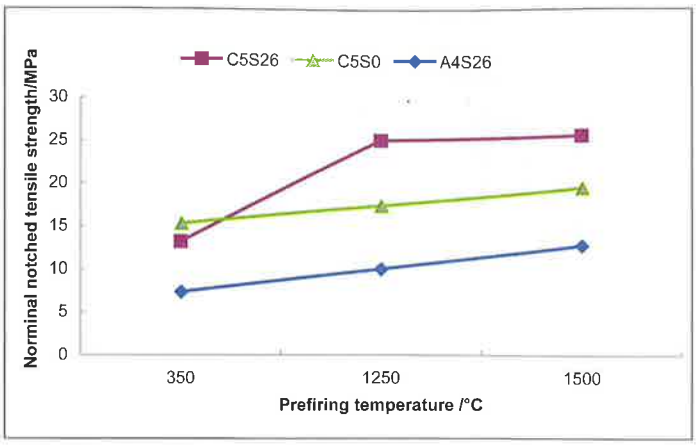

Fig. 20 Nominal notch tensile strength σ_{NT} of castables pre-fired at different temperatures

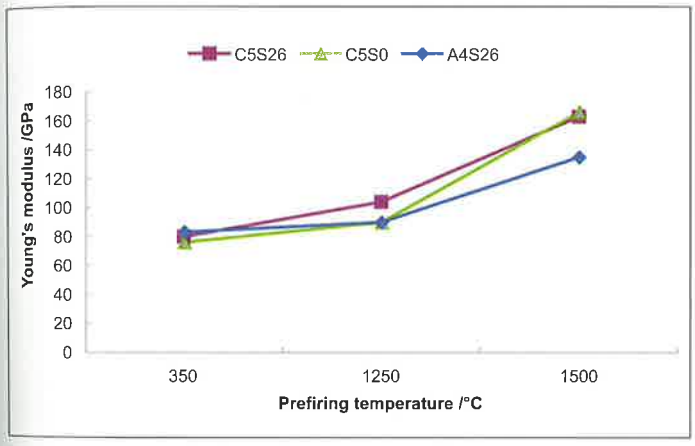

Fig. 21 Young's moduli of castables pre-fired at different temperatures

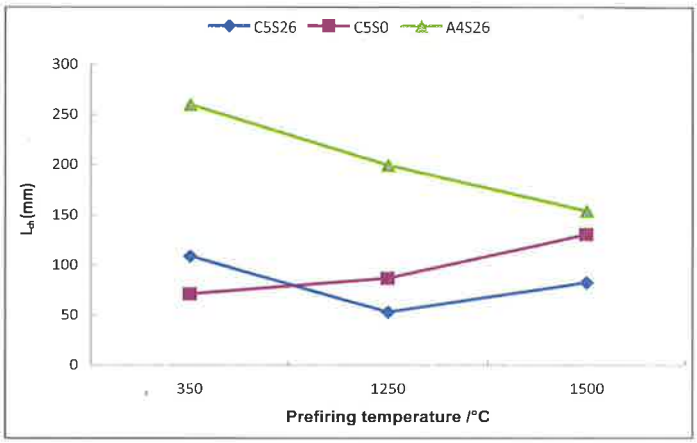

Fig. 22 Characteristic length l_{ch} of castables pre-fired at different temperatures

In the case of castable C5S0, the l_{ch} values are slightly increased with an increase of the pre-firing temperature, because the nominal notch tensile strength is slightly increased with increasing temperature, whilst the Young's modulus E is simultaneously significantly increased. For the two castables C5S0 and C5S26, the l_{ch} slightly increased when the pre-firing temperature was increased from 1250 °C to 1500 °C.

4.4 Microstructural analysis

The microstructures of the different materials after sintering at 1650 °C show distinct differences. The formation of new phases CA_6 and $C_2M_2A_{14}$ in C5S26 is shown in Fig. 23, and EDS and XRD analyses are given in Tab. 4 and Fig. 24 respectively. CA_6 formed dense layers around the sintered corundum grains and $C_2M_2A_{14}$ formed platelets growing into the sintered spinel

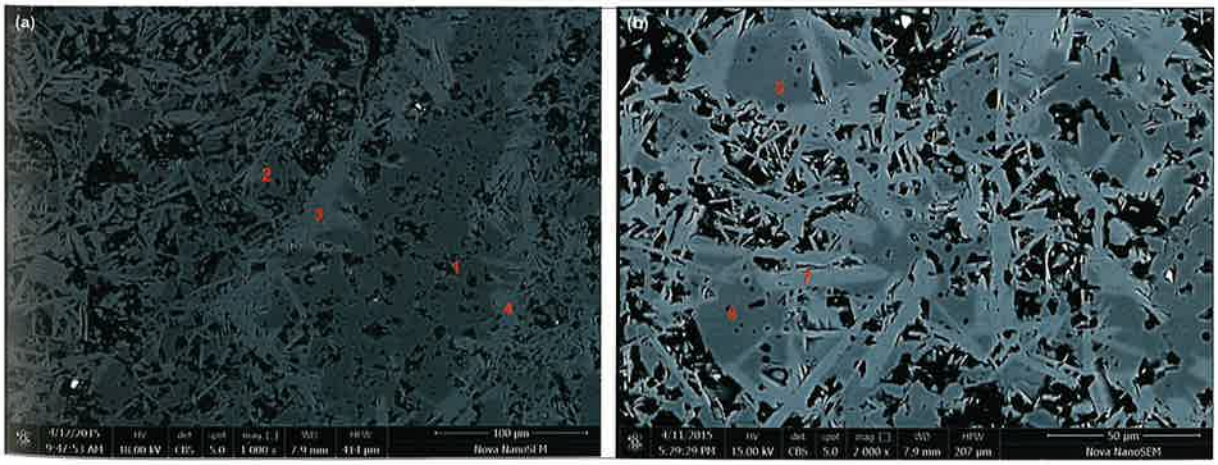

Fig. 23 a–b Microstructure and EDS analysis of C5S26 sintered at 1650 °C for 5 h; EDS analyses are given in Tab. 2

Tab. 4 EDS analysis of C5S26 sintered at 1650 °C for 5 h

Spot	Oxide	[mass-%]	[mol-%]	Intensity [count]	Possible Phase
1	Al_2O_3	100	100	17,889	Corundum
2	MgO	17,7	35,3	3,335	MA spinel
	Al_2O_3	82,2	64,6	13,035	
3	Al_2O_3	91,0	84,7	16,286	CA_6
	CaO	8,9	15,2	1,205	
4	Al_2O_3	91,2	85,1	16,345	CA_6
	CaO	8,7	14,8	1,177	
5	MgO	17,0	34,2	3,124	MA spinel
	Al_2O_3	82,9	65,7	12,897	
6	MgO	17,5	34,9	3,261	MA spinel
	Al_2O_3	82,4	65,0	12,978	
7	MgO	4,9	10,9	871	$C_2M_2A_{14}$
	Al_2O_3	87,9	77,6	14,916	
	CaO	7,1	11,4	938	

grains, intensively interlocking the aggregate grains with the surrounding matrix. CA_6 also formed in C5S0 as platelets in the matrix (Fig. 25), but the interlocking between aggregate grains and the matrix is much lower when compared to the spinel containing formulation.

This microstructural difference could explain the clear difference in hot strength, e.g. HMoR, between cement bonded formulations with and without spinel. And it would also explain the higher specific fracture energy and nominal notch tensile strength of C5S26 when compared to C5S0 after firing at high temperatures. In comparison to the cement bonded materials, the hydratable alumina bonded material A4S26 shows a less densified and more porous microstructure (Fig. 26). During sintering, the transition aluminas from the bond will transform into the thermodynamically stable corundum phase and react with the other fine matrix aluminas.

However, no binary or multicomponent new phases can form and accordingly the interlocking between aggregate grains and matrix is much lower. This explains the lower mechanical strength of the fired no-cement castable when compared to the cement bonded ones.

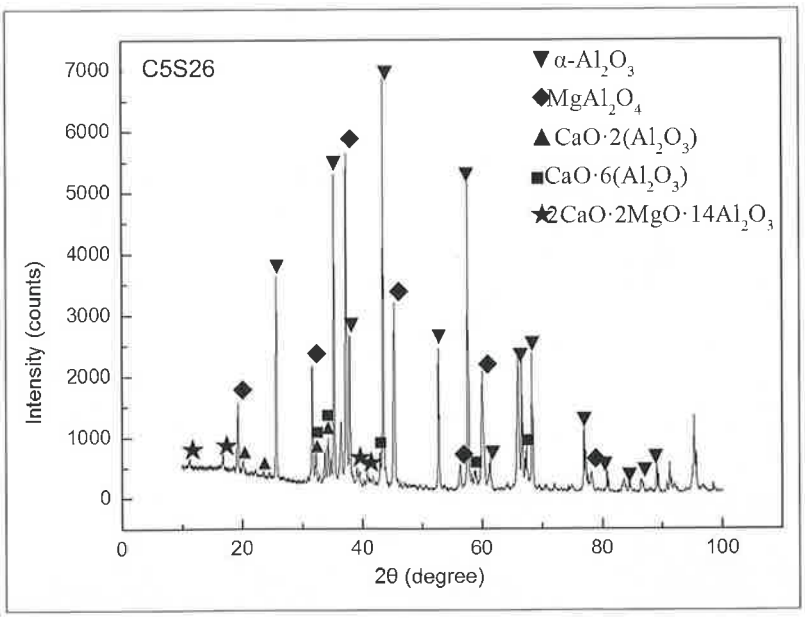

Fig. 24 XRD analysis on C5S26 (pre-fired at 1650 °C for 5 h)

On the other hand, it also explains the ductile, less brittle behaviour of this material during fracture behaviour testing. Crack propagation must be hampered in such a higher porous, less rigidly connected structure. As Sakai et al. described [21], the crack would be deflected by interface de-bonding. In addition, pores could act as the stress arrester, which dismiss the thermal stress by disturbing the route of crack propagation. Because of a much lower nominal notch tensile strength, the thermal shock resistance of the no-cement castable is higher than those of the other two castables.

5 Conclusion

The thermodynamic analysis of the calcia containing system Al_2O_3–MgO–CaO by FactSage, and the calcia-free system Al_2O_3–MgO in contact with iron oxide slag created during the oxygen lancing of purging plug, shows that the calcia-free system provides advantages with regard to melting temperature and the amount of liquid phase formed at a given temperature.

A mixture of 50 mass-% refractory matrix and 50 mass-% iron oxide slag starts melting at 1665 °C for the calcia-free system and at 1575 °C for the calcia containing system. The calcia-free mixture has no liquid at 1600 °C, but the calcia containing mixture has 28 mass-% liquid phase at this temperature.

It can be concluded, that the calcia-free system provides higher corrosion resistance against the iron oxide slag and would be advantageous in this regard when compared to the calcia containing system.

Cement bonded castables show clear differences when compared to hydratable alumina no-cement bonded castables with respect to mechanical properties and fracture behaviour.

The strength as determined by CMoR, CCS, and HMoR at 1500 °C is clearly higher for the cement bonded material. The fracture behaviour as tested with the wedge splitting method shows the no-cement castable to be more ductile and less brittle. The specific fracture energy and nominal notch tensile strength are lower and characteristic length l_{ch} is higher. Also in the usual thermal shock resistance testing by water quenching, the no-cement material shows lower relative strength loss after one and three quenching cycles.

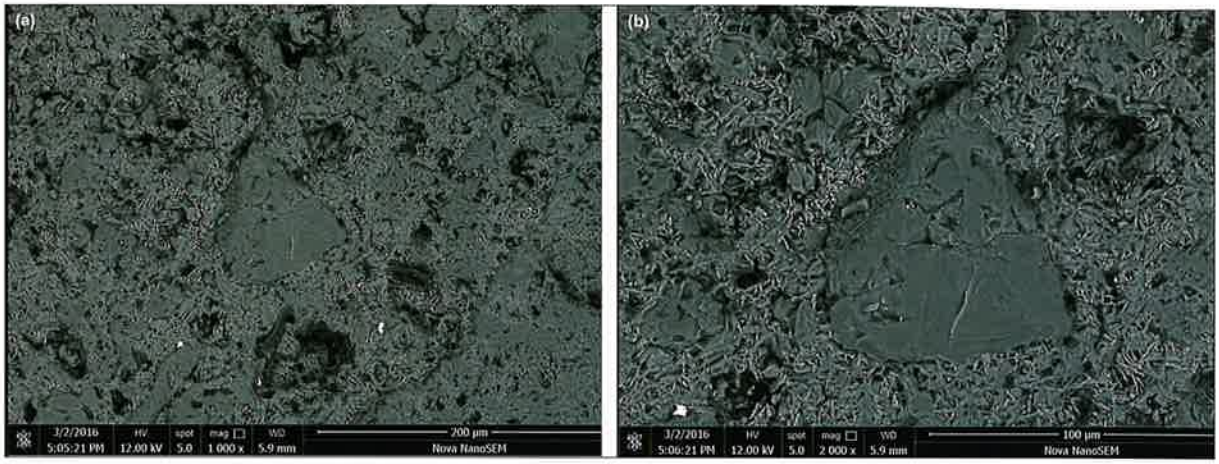

Fig. 25 a–b Microstructure of C5S0 sintered at 1650 °C for 5 h

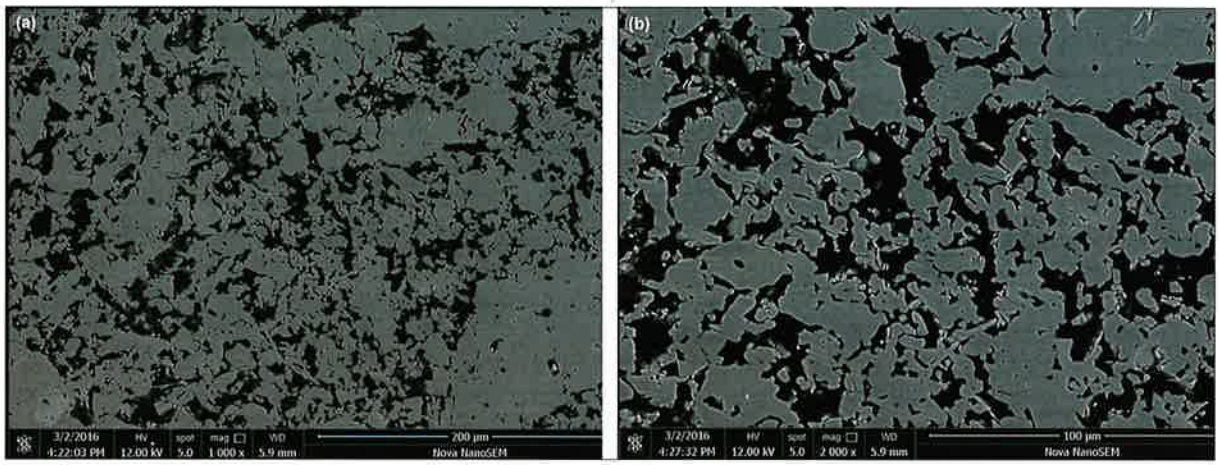

Fig. 26 a–b Microstructure of A4S26 sintered at 1650 °C for 5h

The pre-firing temperature has a clear influence on the strength development and the fracture behaviour of the materials. High pre-firing temperatures of 1500 °C or above enable strong sintering reactions especially in the cement bonded materials, leading to new phase formation in the matrix and different degrees of interlocking between aggregate grains and the matrix. It is most pronounced for the spinel containing cement bonded material due to the ternary phase $C_2M_2A_{14}$ growing from the matrix into the spinel grains.

This would explain the higher hot strength of spinel containing castables when compared to pure corundum castables. With regard to fracture behaviour and resistance against crack propagation, the higher porous, lower strength microstructure of the hydratable alumina castable retains its general characteristic of lower brittleness when compared to the cement bonded materials. From a technical point of view with regard to the application of purging plugs in steel ladles, both binder concepts have advantages and disadvantages.

The established solution with spinel containing low and ultra-low cement castables clearly has higher hot strength, which is favourable for the required erosion resistance during intensive stirring. Regarding the spalling resistance due to thermal cycling, the no-cement system could provide advantages if the overall strength level is high enough for the application.

Such hydratable alumina bonded materials may require pre-firing temperatures of above 1000 °C (e.g. 1250 °C) in order to prevent the low strength which occurs around 1000 °C. Otherwise it may lead to cracking in the body of the purging plug, where temperatures are too low for real sintering reactions.

For cement bonded systems, it is not easy to make a judgement based on the current results if drying at temperatures around 400 °C or pre-firing at e.g. 1600 °C is the best overall solution for the performance of the purging plugs in operation. The fully established, highly sintered microstructure may have advantages for the erosion resistance, but it may be counteracted by higher susceptibility to cracking and spalling. More investigations including extended field trials and an economic assessment of the more expensive high temperature pre-firing route would be necessary in order to finally conclude whether lower or higher pre-firing temperatures are to be recommended for purging plugs.

Based on the results of this investigation it appears to be worthwhile testing such hydratable alumina bonded corundum-spinel materials in industrial applications for steel ladle purging plugs. It would be recommended to pre-fire such hydratable alumina bonded purging plugs at temperatures of min. 1250 °C to ensure sufficient strength for the application.

Acknowledgements

The authors are grateful to Almatis Qingdao for the raw materials and laboratory facilities for testing; Prof. Jung In-Ho from McGill University Canada for the thermodynamic calculations with FactSage; Chair of Ceramics, Montanuniversitaet Leoben/AT, for fracture behaviour testing; and University Science and Technology Beijing/CN for SEM/EDS and XRD testing. This work is a good example of successful scientific cooperation between industrial and academic FIRE-partners from three different continents.

References

[1] Chaudhuri, S.; Stein, D.: Application of new gas purging systems in ladle metallurgy. Interceram (1992) 313–316

[2] Becker, J.U.; et al.: Purging plugs for steel ladles-laboratory and plant results from a BOF steel plant. UNITECR 1997, New Orleans, USA, 143–152

[3] Hiroaki, E.; et al.: Development of long-life slit plug material for steel ladle. UNITECR 1999, Berlin, Germany, 308–311

[4] Zhao, M.: Stirring units for LF/VD ladle in Baosteel. UNITECR 1999, Berlin, Germany, 267–268

[5] Zhang, H.; et al.: Study on ladle purging plug with gradient composite structure and material. UNITECR 2013, Victoria, Canada, 621–624

[6] Long, B.; Buhr, A.; Xu, G.Y.: Thermodynamic evaluation and properties of refractory materials for steel ladle purging plugs in the system Al_2O_3–MgO–CaO. Ceram. Int. **42** (2016) 11930–11940

[7] Long, B.; et al.: Fracture behaviour and microstructure of refractory materials for steel ladle purging plugs in the system Al_2O_3–MgO–CaO. Ceram. Int. **43** (2017) 9679–9685

[8] Tschegg, E.K.: Testing device and appropriate specimen shapes for tests to measure fracture values (in German). Austrian Patent, AT 390328 B, 1990

[9] National Standard on Refractory (CN), 4th ed., China Refractory National Standard Committee, 2010, 35, 59, 43

[10] Harmuth, H.: Stability of crack propagation associated with fracture energy determined by wedge splitting specimen. Theor. Appl. Fract. Mec. **23** (1995) 103–108

[11] Jin, S.; Gruber, D.; Harmuth, H.: Determination of Young's modulus, fracture energy and tensile strength of refractories by inverse estimation of a wedge splitting procedure. Engin. Fract. Mech. **116** (2014) 228–236

[12] Hasselman, H.: Thermal stress resistance parameters for brittle refractory ceramics: a compendium. Ceram Bull. **12** (1970) 1033–1037

[13] Harmuth, H.; Bradt, R.C.: Investigation of refractory brittleness by fracture mechanical and fractographic methods. Interceram (2010) 6–10

[14] National Standard on Refractory (CN), 4th ed., China Refractory National Standard Committee, 2010, 315

[15] Slag Atlas. 2nd ed., Düsseldorf 1995, 104

[16] De Aza, A.H.; Pena, P.; De Aza, A.S.: Ternary system Al_2O_3–MgO–CaO: Part 1, primary phase field of crystallization of spinel in the subsystem $MgAl_2O_4$–$CaAl_4O_7$–CaO–MgO. J. of Amer. Ceram. Soc. **82** (1999) 2193–2203

[17] De Aza, A.H.; et al.: Ternary system Al_2O_3–MgO–CaO: part 2. Phase relationships in the subsystem Al_2O_3–$MgAl_2O_4$–$CaAl_4O_7$. J. of Amer. Ceram. Soc. **83** (2000) 919–927

[18] Göbbels, M.; Woermann, E.; Jung, J.: The Al-rich part of the system CaO–Al_2O_3–MgO, Part I: Phase relationships. J. of Solid State Chemistry **120** (1995) 358–363

[19] Iyi, N.; Göbbels, M.; Matsui, Y.: The Al-rich part of the system CaO–Al_2O_3–MgO, Part II: Structure refinement of two new magnetoplumbite-related phases. J. of Solid State Chemistry **120** (1995) 364–371

[20] Lide, D.R.: Handbook of Chemistry and Physics, 73rd ed. (1992–1993), Boca Raton, FL, 5–18

[21] Sakai, M.; Bradt, R.C.: Fracture toughness testing of brittle materials. Int. Mater. Rev **38** (1993) [2] 53–78